International Journal of Hydrogen Energy 92 (2024) 1069–1077

Contents lists available at ScienceDirect

International Journal of Hydrogen Energy

journal homepage: www.elsevier.com/locate/he

Strain engineering for optimized hydrogen storage: Enhancing ionic conductivity and achieving near-room-temperature desorption in Mg_2NiH_4

Amine Alaoui-Belghiti [a,*], Abdelmajid Assila [a,**], Ikram Belkoufa [a], Mourad Rkhis [a,b], Said Laasri [a], Mouhaydine Tlemçani [c], El-kebir Hlil [d], Abdelowahed Hajjaji [a]

[a] Chouaib Doukkali University of El Jadida, National School of Applied Sciences, Engineering Sciences for Energy Lab, El Jadida, Morocco
[b] Research Institute for Solar Energy and New Energies (IRESEN), Morocco
[c] Department of Mechatronics Engineering, School of Science and Technology, Universidade de Évora, Colégio Luis António Verney, Rua Romão Ramalho, N° 59, 7000–671, Évora, Portugal
[d] Univ. Grenoble Alpes, CNRS, Grenoble INP, Institut Neel, 38000, Grenoble, France

ARTICLE INFO

Handling Editor: Dr F Gallucci

Keywords:
Hydrogen
Magnesium
Hydride
DFT
Conductivity
Mechanical properties

ABSTRACT

This study investigates strain engineering to optimize hydrogen storage in Mg_2NiH_4, with a focus on enhancing ionic conductivity and approaching room-temperature desorption. Using density functional theory (DFT), we analysed the effects of uniaxial and biaxial tensile and compressive strains on the structural, mechanical, diffusion kinetics, and electronic properties of Mg_2NiH_4. The activation energy for hydrogen diffusion was found to range from 0.38 to 0.45 eV under different strain conditions. The application of strain significantly influences ionic conductivity, with uniaxial strain resulting in values between 1.18 and 25.5 S/m, and biaxial strain yielding values from 12.3 to 18.3 S/m. Mechanical analysis shows that Mg_2NiH_4 exhibits brittle behaviour across all strain conditions. Additionally, electronic structure analysis indicates that the material maintains its metallic properties under both uniaxial and biaxial strain. Although the study did not achieve room-temperature desorption, it demonstrated significant progress, with desorption occurring at approximately 500 K. These results demonstrate that strain engineering can significantly improve ionic conductivity and facilitate hydrogen desorption closer to practical room temperature, providing valuable insights for optimizing Mg_2NiH_4 for practical hydrogen storage applications.

1. Introduction

As an energy carrier, hydrogen is increasingly attracting attention from researchers to develop new materials, as it plays a key role in the transition to a sustainable energy future [1–11]. Fossil fuels, such as gas, coal, and oil, are rapidly approaching depletion [12,13]. This depletion will be accelerated as the population grows, and the faster this growth occurs, the sooner the available fossil fuel reserves will be exhausted [12,14–16]. Indeed, population growth demands greater energy resources to support development and improve daily living conditions [17,18]. This increased demand contributes significantly to greenhouse gas emissions, leading to environmental crises and a world burdened by heightened levels of disease [14,19].

In fact, there are other types of energy, such as solar, wind and hydraulic power [20,21]. While these energies are less polluting, they do present another challenge, namely temporal sustainability [17,22]. For example, on cloudy days, solar production is significantly reduced. Similarly, if the wind speed isn't between 4 m/s and 25 m/s, wind turbines don't produce energy, as they need this specific range to be effective [21,23]. What's more, in periods of drought, when dams are empty, hydropower generation is halted [21,23]. Faced with these major challenges, hydrogen is an effective solution, thanks to its numerous advantages, including high energy density, low environmental impact, and long-term sustainability [22,24–29]. For example, 11% of the ocean's mass is composed of hydrogen. When used, hydrogen combines with oxygen to produce water, further enhancing its role in reducing greenhouse gas emissions [18,30,31].

However, hydrogen storage remains a major obstacle in the energy field. As several research projects have pointed out, hydrogen solid-state storage can solve volume-related issues, as hydrogen would be stored

* Corresponding author.
** Corresponding author.
E-mail addresses: alaouibelghiti.a@ucd.ac.ma (A. Alaoui-Belghiti), assila.a@ucd.ac.ma (A. Assila), laasri.s@ucd.ac.ma (S. Laasri).

https://doi.org/10.1016/j.ijhydene.2024.10.292
Received 18 September 2024; Received in revised form 18 October 2024; Accepted 20 October 2024
Available online 29 October 2024

within the material itself rather than in a tank, where it occupies a large volume with low energy density [19,32]. Although hydrogen storage is not reversible in all existing materials, it is preferable to work with reversible hydrides to fully utilize the stored hydrogen [33,34]. Several industrial and academic laboratories have recently published results on the development of highly resistant tanks capable of operating at pressures of 700 bar and storing 30 kg of hydrogen per cubic meter [18,31]. Despite this great progress, there is still a need to improve safety to mitigate the risk of explosion, particularly when using these tanks for transport [33,35,36]. There are also other forms of hydrogen storage, such as liquid hydrogen storage, where hydrogen is cooled to 20 K, which presents a major technical challenge for this type of storage [16, 37].

Indeed, these major problems pose significant challenges that must be addressed to meet the world's growing energy demand [38–40]. Among the most promising solutions is hydrogen solid-state storage (HSSS), which involves storing hydrogen molecules (H_2) either on the surface of carefully selected materials or within the interstitial sites of these materials [34]. Generally, materials capable of storing hydrogen, known as hydrides, are not immediately recognized as hydrogen storage systems. According to the US Department of Energy (DOE), a hydride is categorized as a suitable hydrogen storage material if it has a formation enthalpy $\Delta H = -40$ kJ/molH_2 and operates at ambient temperature [41, 42]. To date, several research projects have theoretically validated these criteria. For example, previously published results have studied hydrides such as MgH_2, $ZrNiH_3$, and $LiBH_4$ [19,43–45]. Additionally, due to its gravimetric hydrogen capacity of 3.6% and its portability, the Mg_2NiH_4 hydride with space group (*C2/m*) is considered as an acceptable material for hydrogen storage [18].

In this work, we investigate the structural, thermodynamic, mechanical, hydrogenation kinetics, ionic conductivity, and electronic properties of the hydride Mg_2NiH_4 under uniaxial and biaxial tensile and compressive strains using density functional theory (DFT), based on the generalized gradient approximation for solids developed by Perdew-Burke-Ernzerhof (GGA-PBEsol) [30,46]. Our primary objectives are to first validate the structural properties by comparing them with existing literature, and then to explore the mechanical properties. Subsequently, we apply uniaxial and biaxial tensile/compressive strains to examine the hydrogenation kinetics and ionic conductivity of the Mg_2NiH_4 hydride. This study goes beyond the previously published work [18].by providing a comprehensive analysis of the mechanical, electronic, and diffusion properties, alongside a detailed investigation into ionic conductivity and hydrogen desorption kinetics of Mg_2NiH_4 under uniaxial and biaxial strain. To the best of our knowledge, this work represents the first study on the improvement of ionic conductivity and the mechanical behaviour of the Mg_2NiH_4 system under uniaxial/biaxial strain, as no prior research has been conducted in this area. We believe the results obtained from our study could pave the way for new advancements in the development of hydrogen storage systems, as well as the application of ionic conductivity under uniaxial/biaxial strain in other fields.

2. Computational approach and methods

The calculations performed during this work were carried out using the Cambridge Serial Total Energy Package (CASTEP) calculation code [47]. All calculations are based on density functional theory (DFT), using generalized gradient approximations improved by Perdew-Burke-Ernzerhof for solids (GGA-PBEsol) and (GGA-PBE) [25, 46,48]. In order to optimize the structural, thermodynamic, mechanical, diffusion kinetics, ionic conductivity and electronic properties of the Mg_2NiH_4, Mg_2Ni systems and the H_2 hydrogen molecule, we chose ultrasoft pseudopotentials with a $7 \times 7 \times 4$ K-point grid and a cutoff energy of 380 eV [19,33]. The convergence criteria for maximum displacement, maximum force, maximum strain and energy per atom are 5×10^{-4} Å, 0.01 eV/Å, 0.02 GPa and 5×10^{-6} eV/atom respectively.

The Mg_2NiH_4 structure is subjected to tensile/compressive uniaxial and biaxial strains with a 4% step along the *Oz* axis in the [001] direction for uniaxial strains, and along *Ox* and *Oy* in the [100] and [010] directions simultaneously for biaxial strains [18,33,44,45]. The mathematical equations governing the uniaxial and biaxial strain applied to the Mg_2NiH_4 hydride system are formulated as follows:

$$\varepsilon_{zz}(\%) = \frac{c - c_0}{c_0} \times 100\% \quad \textit{uniaxial strain}$$

$$\varepsilon_{xx}(\%) = \varepsilon_{yy}(\%) = \frac{a(b) - a_0(b_0)}{a_0(b_0)} \times 100\% \quad \textit{biaxial strain}$$

a_0, b_0 and c_0 are the mesh parameters of the unstrained Mg_2NiH_4 system, while a, b and c are the mesh parameters of the optimized Mg_2NiH_4 system. Positive values correspond to tensile strains, while negative values correspond to compressive strains. Fig. 1 models these strains as follows.

3. Results and discussion

3.1. Structural properties

Mg_2NiH_4 undergoes a phase transformation between 240 °C and 210 °C, transitioning from a high-temperature (HT) cubic phase (Fm-3m) to a low-temperature monoclinic (LT) phase [49,50]. The cubic HT phase adopts an antifluoride-type structure (space group: Fm3m). However, the crystal structures of the LT phases remain somewhat ambiguous. At least two monoclinic LT hydride phases have been reported: one with space group *C2/c* (a = 14.343 Å, b = 6.4038 Å, c = 6.4864 Å, and β = 113.520°) and another with space group *C2/m* (a = 6.497 Å, b = 6.414 Å, c = 6.601 Å, and β = 93.23°) [50–52].

Hydrogen atoms in crystals contribute weakly to X-ray diffraction (DRX), making their positions difficult to determine. Neutron diffraction, as used by Noréus et al. [51,53], is often employed to extract accurate hydrogen atom positions. Their study provided valuable insights into the *C2/m* phase of Mg_2NiH_4, stable below 235 °C, which aligns with the temperature range used in this work. The *C2/m* space group was chosen because it offers stable metallic properties, which are critical for studying the strain effects on the mechanical, electronic, and hydrogen storage properties of Mg_2NiH_4, with a specific focus on achieving near-room-temperature hydrogen desorption.

To ensure accurate results, we first optimized the parameters for the Mg_2NiH_4 hydride meshes before analyzing their elastic properties, thermodynamics, diffusion kinetics, ionic conductivity, and structural characteristics. The optimized parameters of the primitive cell, calculated using the GGA-PBEsol approximation, are $a_0 = b_0 = 4.45$ Å and $c_0 = 8.96$ Å, These values are in excellent agreement with those reported in the literature, where GGA-PBE, GGA-WC, and LDA-CA-PZ approximations yielded: a = b = 4.49 Å and c = 9.05 Å, a = b = 4.45 Å and c = 8.97 Å, a = b = 4.39 Å and c = 8.85 Å [18].

3.2. Volume

Since hydrides are generally formed by the alloying of a metal with hydrogen, their volume can fluctuate under tensile and compressive strains due to the diffusion of hydrogen atoms. The study of volume changes in hydrides is crucial to understanding how they respond to applied strains, which is valuable for guiding industry in the development of explosion-resistant proton exchange membrane (PEM) fuel cells and hydrogen storage/release systems [54]. For the Mg_2NiH_4 hydride, the volume variations under tension and compression are illustrated in the diagram in Fig. 1.

Since hydrides in general are formed by the alloying of a metal with hydrogen, their volume can vary during tensile/compressive strains due to the diffusion of hydrogen atoms. Moreover, the interest in studying the volume of hydrides lies in knowing how they react to the strains

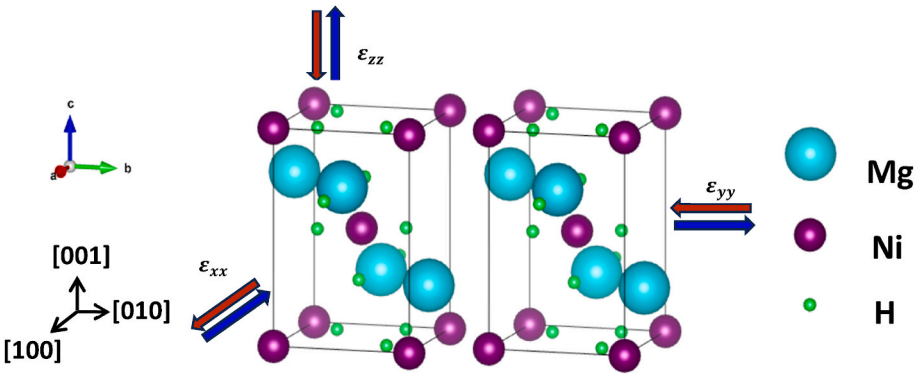

Fig. 1. Schematic of Mg_2NiH_4 systems under uniaxial and biaxial strain.

applied to them. This can guide industry in the development of explosion-resistant fuel cells (PEM) and hydrogen storage/release systems [54]. For Mg_2NiH_4 hydride, the volume variation under tensile/-compressive strain is depicted in Fig. 1.

As illustrated in Fig. 2, the volume of free Mg_2NiH_4 hydride is 177.20 $Å^3$, which is in excellent agreement with values reported in the literature using the generalized gradient approximation developed by Perdew-Burke-Ernzerhof (GGA-PBE), yielding 182.42 $Å^3$ [18]. Based on the generalized gradient approximation for solids (GGA-PBEsol), the system volume exhibits a linear variation under tensile and compressive strains. Specifically, the hydride volume decreases to 162.95 $Å^3$ and 150.04 $Å^3$ under uniaxial and biaxial compressive strain, respectively, with a strain $\varepsilon = -8\%$. This reduction in volume can be attributed to several factors, including the decreased atomic spacing, diffusion of hydrogen atoms into neighbouring sites, and variations in the total energy of the Mg_2NiH_4 system. In contrast, the volume expands under uniaxial and biaxial strain by 8%, increasing to 193.5 $Å^3$ and 207.17 $Å^3$, respectively. This underscores the importance for proton exchange membrane (PEM) fuel cell manufacturers to account for this volume increase to prevent potential damage to the cell [33,54]. To further our understanding of rigidity and safety during hydrogen storage and release, we next investigated the elastic properties of the Mg_2NiH_4 system.

3.3. Thermodynamic properties

To investigate the ionic conductivity during the hydrogenation process, it is essential to determine the decomposition temperature T of

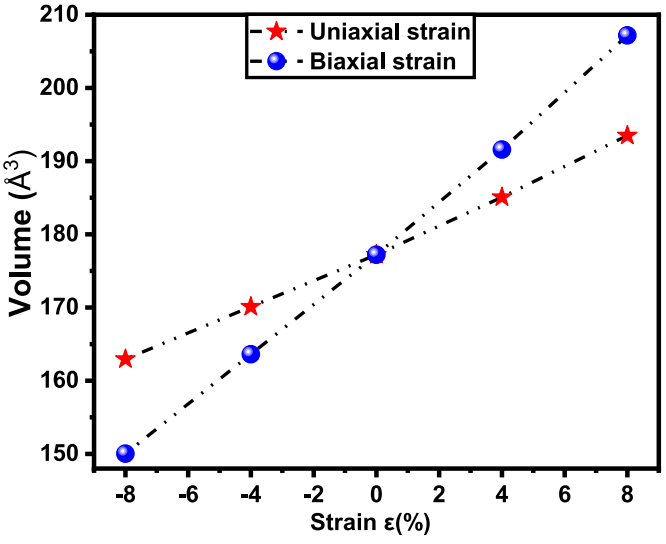

Fig. 2. Volume change of Mg_2NiH_4 system under tensile/compressive strain.

the Mg_2NiH_4 system under various strain conditions, including uniaxial, biaxial, and zero strain. To the readers' knowledge, in this section, the Perdew-Burke-Ernzerhof (PBE) approximation will be employed to accurately model the effects of strain on the decomposition temperature, as it has been demonstrated to provide reliable results consistent with experimental data. This requires calculating the enthalpy of formation ΔH_f. The calculation of the enthalpy of formation and decomposition temperature is based on the following reaction equation (***equation (1)***) for the formation of Mg_2NiH_4 [18,40]:

$$Mg_2Ni + 2H_2 \leftrightarrow Mg_2NiH_4 \quad (1)$$

The enthalpy of formation is calculated by optimizing the total energies of the Mg_2NiH_4, Mg_2Ni, and H_2 (hydrogen molecule) systems. As outlined in several studies, it is defined as the difference between the total energy of the products and that of the reactants (***equation (2)***). [43,44].

$$\Delta H_f = E_t(Mg_2NiH_4) - E_t(Mg_2Ni) - 2E_t(H_2) \quad (2)$$

The calculated enthalpy of formation for the unstrained Mg_2NiH_4 system, using both the GGA-PBE and GGA-PBEsol approximations, was found to be −69.97 kJ/molH_2 and −72.37 kJ/molH_2, respectively. These computational results are in excellent agreement with experimental data, which report formation enthalpies of −72.85 kJ/molH_2, −63.04 kJ/molH_2, −64.5 kJ/molH_2, −64.0 kJ/molH_2, and −63.42 kJ/molH_2 [27,55,56]. Following this step, the decomposition temperature is determined using Van't Hoff's law (***equation (3)***) [19,25,30]:

$$\Delta G = \Delta H_f - T\Delta S \quad (3)$$

With ΔG the standard Gibbs energy and ΔS the entropy of reaction, in the case of metal hydrides, the entropy is equal to 130 J/mol.K [31,45]. If the system were at equilibrium, the standard Gibbs energy would be equal to 0 J/mol [31,44]. Consequently, the decomposition temperature would be equal to:

$$T = \frac{\Delta H_f}{\Delta S} \quad (4)$$

Based on this equation, the temperature of the unstrained hydride is equal to 556,69 K. which is in good agreement with literature results of 593 K [55]. The mechanism by which tensile and compressive strains affect the enthalpy of formation and decomposition temperature lies in the change in atomic spacing and interaction energy within the Mg_2NiH_4 lattice. Compressive strain brings atoms closer together, increasing the system's internal energy and thus lowering the formation enthalpy, while tensile strain has the opposite effect. These atomic-level interactions also influence the stability of hydrogen within the structure, leading to changes in the decomposition temperature. These atomic-level modifications induced by strain are critical for altering the hydrogen storage characteristics of the material.

To summarize the calculated values of formation enthalpy and

decomposition temperature under different strain conditions, we present them in Table 1.

3.4. Activation energy

Knowing the activation energy can facilitate the selection of appropriate materials for hydrogen storage. Specifically, a lower activation energy indicates a faster and more efficient hydrogenation process. Activation energy is defined as the energy difference between the initial and final states during the migration of H^- ions from one site to a nearby site.

As illustrated in Fig. 3, the activation energy for the free Mg_2NiH_4 hydride is approximately 0.4 eV. This energy varies with the applied strain. Specifically, under maximum uniaxial tension of +8%, the activation energy peaks at about 0.45 eV, whereas it reaches a minimum of 0.38 eV under uniaxial compression of −8%. This phenomenon was also observed in other research using approximations (GGA-PBE) [18], which reported activation energies ranging from 0.22 eV to 0.4 eV, consistent with our findings. This variation in the activation energy of the Mg_2NiH_4 system can be explained by the variation in internal energy during tensile/compressive strains and also by the variation in distance between neighbouring sites. These findings could pave the way for further research into ionic conductivity, as H^- ions migrate through the material under strain.

3.5. Ionic conductivity

Following the study of activation energy, further research was conducted to examine the influence of strain on the ionic conductivity of Mg_2NiH_4 hydride. This conductivity, which occurs as H^- ions migrate from one site to a nearby site, is influenced by various factors including decomposition temperature, ion concentration, the material's crystal structure, and other properties specific to the solid [57–59]. Thanks to their unique ionic conductivity properties, metal hydrides are widely used in applications such as fuel cells, batteries, sensors, electronic devices and energy systems. Conductivity is defined as follows [60–62]:

$$\sigma = \frac{2}{3}\left[\frac{(Ze)^2}{kTm} n E_a \tau_0 \exp\left(\left[\frac{-E_a}{kT}\right]\right)\right]$$

With Ze the charge of the H^- ion, K the Boltzmann constant, T the decomposition temperature, m the molar mass of the H^- ion, n the number of hydrogen atoms per mesh, E_a the activation energy, τ_0 the hydrogen atom displacement temp from one site to the nearest neighbouring site. It should be noted that the study was carried out in the following cases.

Table 1
Thermodynamic properties of Mg_2NiH_4 under uniaxial and biaxial strain steps.

Strain			Formation enthalpy (Kj/mol. H_2)	Decomposition temperature (K)
Uniaxial	Tensil	ε = +8%	−60,80	467.68
		ε = +4%	−69,29	532,98
	Compression	ε = −8%	−58,81	452.41
		ε = −4%	−69,01	530,87
Biaxial	Tensil	ε = +8%	−37.25	286,55
		ε = +4%	−62,28	479,11
	Compression	ε = −8%	−33,83	260,24
		ε = −4%	−63,39	487,60

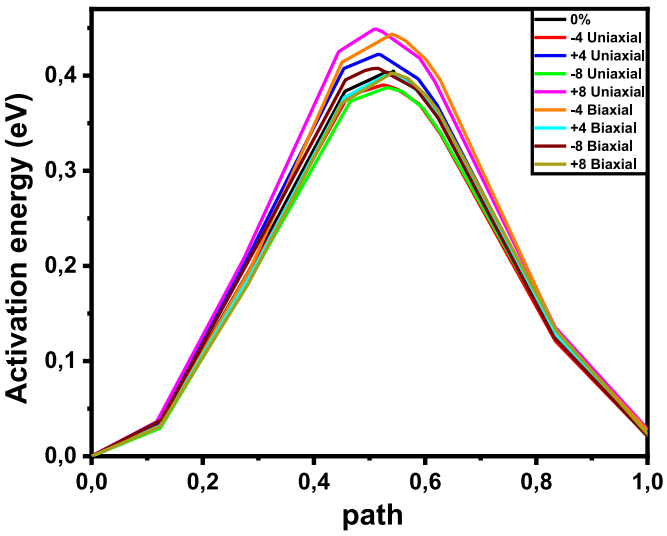

Fig. 3. Activation energy of the free Mg_2NiH_4 system, and under uniaxial/biaxial strain.

✓ Mg_2NiH_4 hydride is subjected to no strain.
✓ Mg_2NiH_4 hydride is subjected to tensile/compressive strains ε = ±4% and ε = ±8% uniaxial and biaxial.

The results are shown in Fig. 4.

Fig. 4, shows that the ionic conductivity of the hydride Mg_2NiH_4 is modified by increasing uniaxial/biaxial strains, due to variations in the hydride's thermodynamic and structural properties. Noting that the nearest neighbor sites lie in the [001] direction, i.e. in the *Oz* axis direction, in the equation the distance between two hydrogen atoms under free strain is 2.183 Å. More precisely, under free strain, conductivity is equal to 21.8 S/m and under maximum tension ε = +8%, uniaxial/biaxial, it decreases to 1.18 S/m and 14 S/m respectively. This is due to

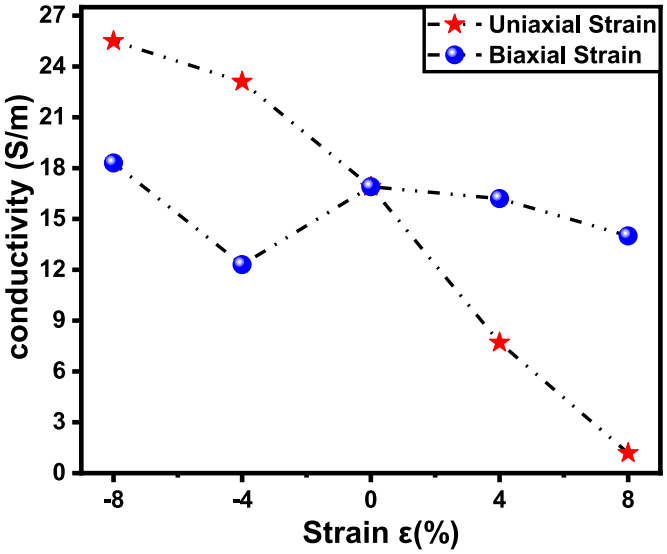

Fig. 4. Diagram of Mg_2NiH_4 hydride conductivity variation as a function of strain.

the fact that when uniaxial tensile stresses are applied, the distance between two neighbouring atoms increases to 2.237 *Å*, corresponding to an increase of 2.41% compared to the distance between two neighbouring atoms in the free Mg_2NiH_4 system. On the other hand, this distance increases slightly under biaxial traction, reaching 2.186 *Å*, an increase of 0.14% compared to the free Mg_2NiH_4 system. On the other hand, during maximum compression $\varepsilon = -8\%$ uniaxial/biaxial, conductivity increases to 25.5 *S/m* and 18.3 *S/m*, respectively. This increase in conductivity during compression can be explained either by a decrease in the distance between neighbouring atoms, or by a reduction in activation energy. Specifically, under uniaxial strain, although the distance between sites increases to 2.185 Å, conductivity rises due to a decrease in activation energy, which is estimated to be around 0.38 eV. Conversely, under maximum biaxial compression, conductivity also increases because the distance between neighbouring atoms decreases to 2.182 Å compared to the free Mg_2NiH_4 system. This study clearly demonstrates that compressive strains, both uniaxial and biaxial, significantly enhance ionic conductivity compared to tensile strains. However, under biaxial compression of $\varepsilon = -4\%$, conductivity decreases.

Under uniaxial tensile strain, the significant reduction in conductivity is primarily due to the increased atomic spacing along the strained axis, which weakens electron mobility. As the lattice stretches, the overlap between electron orbitals is reduced, disrupting electron pathways and resulting in a sharp decline in conductivity, as seen in the red curve in Fig. 4 at positive strain values. In contrast, when uniaxial compressive strain is applied (negative strain values), the reduction in atomic spacing enhances electron interactions, leading to an increase in conductivity. This underscores the sensitivity of Mg_2NiH_4's conductivity to changes in atomic spacing and strain-induced modifications in the electronic structure, particularly under tensile strain.

The contrasting behaviour of electrical conductivity under uniaxial and biaxial strain can be attributed to the anisotropic vs. isotropic nature of the applied strain. Under uniaxial strain, the lattice distortion occurs along a single axis, leading to more significant changes in the electronic density of states (DOS) and a pronounced impact on electron mobility. This results in sharper fluctuations in conductivity, as reflected by the red curve in Fig. 4. Conversely, biaxial strain distributes the deformation more evenly across two perpendicular axes, resulting in smoother, more gradual changes in the DOS and thus more stable conductivity, as seen in the blue curve in the same figure. The strain-induced changes in atomic spacing and electronic structure are therefore much more pronounced under uniaxial strain, explaining the non-linear, more drastic changes in conductivity.

3.6. Mechanical properties

To assess the suitability of a hydride for hydrogen storage applications, it is crucial to examine its mechanical stability. Specifically, for studying the mechanical stability of hydrides such as the monoclinic Mg_2NiH_4 structure (space group *C*2/*m*, No. 12), it is essential to validate several criteria, including the following [63]:

$C_{11} > 0, C_{22} > 0, C_{33} > 0, C_{44} > 0, C_{55} > 0, C_{66} > 0,$

$C_{11}+C_{22}+C_{33}+2(C_{12}+C_{13}+C_{23})>0,$

$C_{33}C_{55}-C_{35}^2 >0,$

$C_{44}C_{66}-C_{46}^2>0,$

$C_{22}+C_{33}-2C_{23} > 0,$

It is important to note that no prior research has been conducted on the mechanical stability of Mg_2NiH_4 hydride. As such, the results of this study are expected to contribute meaningfully to future investigations [27]. The following matrix summarizes the calculation of the elastic constants C_{ij} for Mg_2NiH_4 hydride, and clearly demonstrates the validity of the stability criteria.

$$C_{ij} = \begin{pmatrix} 124.36095 & 46.13617 & 34.44678 & 0.00000 & -0.70330 & 0.00000 \\ 46.13617 & 143.90940 & 47.84325 & 0.00000 & 1.67730 & 0.00000 \\ 34.44678 & 47.84325 & 123.33190 & 0.00000 & -0.79255 & 0.00000 \\ 0.00000 & 0.00000 & 0.00000 & 36.44375 & 0.00000 & -3.70013 \\ -0.70330 & 1.67730 & -0.79255 & 0.00000 & 49.63645 & 0.00000 \\ 0.00000 & 0.00000 & 0.00000 & -3.70013 & 0.00000 & 36.65380 \end{pmatrix}$$

The next step is to evaluate how a material responds to tensile and compressive strains as well as pressure changes. This involves examining elastic coefficients such as the compressibility modulus ***K***, shear modulus ***G***, and Young's modulus ***E***, along with Poisson's ratio ν and the principal Lamé constant λ. A material is typically regarded as rigid if it exhibits a very high Young's modulus. The shear modulus ***G*** measures a material's resistance to transverse strains, while the compressibility modulus ***K*** assesses resistance to volume changes, which is a fundamental physical property of solids. Both the compressibility modulus ***K*** and shear modulus ***G*** can be used to predict whether a material is brittle or ductile. Specifically, several studies suggest that the ratio of the isostatic modulus to the shear modulus (***K/G***) can indicate this characteristic: if ***K/G*** is greater than 1.75, the material is considered ductile, whereas if it is less than 1.75, the material is deemed brittle [44,64]. The Poisson's ratio ν is defined as an important factor for measuring the relationship between transverse and longitudinal strains of a material under strain, while the principal Lamé constant λ is calculated to describe the elastic behaviour of the Mg_2NiH_4 system.

In 1928, Voigt proposed a method for calculating elastic constants, in which he assumed that the material was homogeneous and that strains were uniform throughout the material [63]. Following this assumption, in 1929 Reuss proposed a deferential method in which the material is perfectly bonded, with all phases subjected to the same strain when a force is applied [65]. Another method, proposed in 1952 by Hill, assumes that the composite material is sufficiently homogeneous on a macroscopic scale to use a weighted average of the properties of the constituent phases [66]. This method is also known as the Voigt-Reuss-Hill (VRH) method. Based on these assumptions, the elastic coefficients are determined by the following equations:

According to Voigt's averaging scheme (upper bound):

Bulk modulus: $K_V=(1/9)[(C_{11}+C_{22}+C_{33})+2(C_{12}+C_{23}+C_{31})]$

Shear modulus: $G_V=(1/15)[(C_{11}+C_{22}+C_{33})-(C_{12}+C_{23}+C_{31})+3(C_{44}+C_{55}+C_{66})]$

According to Reuss averaging scheme (lower bound):

Bulk modulus: $1/K_R=(S_{11}+S_{22}+S_{33})+2(S_{12}+S_{23}+S_{31})$

Shear modulus: $15/G_R = 4(S_{11}+S_{22}+S_{33})-4(S_{12}+S_{23}+S_{31})+3(S_{44}+S_{55}+S_{66})$

According to Average Voigt-Reuss-Hill (VRH):

Bulk modulus: $K_{VRH}=(K_V + K_R)/2$

Shear modulus: $G_{VRH}=(G_V + G_R)/2$

The Young's modulus ***E***, Poisson's ratio ν and principal Lamé constant λ are determined by the following equations under the three assumptions.

Young's modulus: $E=(9\,KG)/(3K + G)$

Isotropic Poisson's ratio: $\nu =(3K-E)/(6K)\equiv(3K-2G)/(2(3K + G))$

Lame's first parameter: $\lambda = \nu E/(1 + \nu)(1-2\nu)$

The results of the calculation are summarized in Table 2:

The results presented in Table 2 indicate that the *K/G* ratios, calculated using the Voigt, Reuss, and Hill approximations, are 1.71, 1.72, and 1.71, respectively. These values suggest that the Mg_2NiH_4 system

Table 2
Elastic coefficients of the Mg_2NiH_4 system.

	Voigt	Reuss	Hill
Bulk modulus	72.05052	71.13492	71.59272
Shear modulus (lame mu)	42.09187	41.18694	41.63941
Lame lambda	43.98927	43.67696	43.83311
Young modulus	105.69357	103.57159	104.63287
Poisson ratio	0.25551	0.25734	0.25642

exhibits brittle characteristics. Furthermore, the high Young's modulus values derived from the Voigt, Reuss, and Voigt-Reuss-Hill approximations confirm that the Mg_2NiH_4 system demonstrates considerable resistance to the applied strains.

To investigate the thermal behaviour of the Mg_2NiH_4 system and analyze the normal modes of vibration of the crystal, it is necessary to examine the Debye temperature, θ_D [63]. The Debye temperature is a critical thermophysical parameter in solids, facilitating the correlation between various physical properties. For example, it helps explain activation energy, decomposition temperature, enthalpy of formation, ionic conductivity, as well as the thermal temperature and bonding forces between atoms in the Mg_2NiH_4 system. This temperature is defined by equation (5):

$$\theta_D = V_m \sqrt[3]{\frac{h}{k}\left[\left(\frac{3N}{4\pi}\right)\frac{N_A\rho}{M}\right]} \tag{5}$$

Where V_m is the mean velocity of sound, h is Planck's constant, K is Boltzmann's constant, N is the number of atoms in the unit cell, N_A is Avogadro's number and M is the molar mass of the Mg_2NiH_4 system. The mean velocity Vm is defined by equation (6) [63]:

$$V_m = \frac{1}{\sqrt[3]{\left[\frac{1}{3}\left(\frac{2}{V_t^3}+\frac{1}{V_l^3}\right)\right]}} \tag{6}$$

Where $V_t = \sqrt{\frac{G}{\rho}}$ and $V_l = \sqrt{\frac{3B+4G}{3\rho}}$.

Based on these equations, the calculated sound velocity V_l is of the order of 4224.32 m/s, indicating that the atoms in the Mg_2NiH_4 system can vibrate at high frequencies. Consequently, the Debye temperature is estimated at 600.36 K.

3.7. Density of state

In the field of hydrogen storage, analyzing the Partial Density of States (PDOS) and Total Density of States (TDOS) can offer valuable insights into the variation of thermodynamic properties and the kinetics of hydrogenation processes. This approach is particularly useful for understanding how uniaxial and biaxial strain affect the hydrogenation behaviour, as the electronic structure modifications revealed by PDOS and TDOS play a key role in governing the energy landscape and diffusion pathways of hydrogen atoms [19,45]. As previously reported in several studies, the application of strain or the substitution of chemical elements in the system can lead to significant variations in the Fermi level and alter the contribution of specific orbitals. These changes can influence the electronic structure and, consequently, the material's thermodynamic and kinetic properties, particularly in systems such as

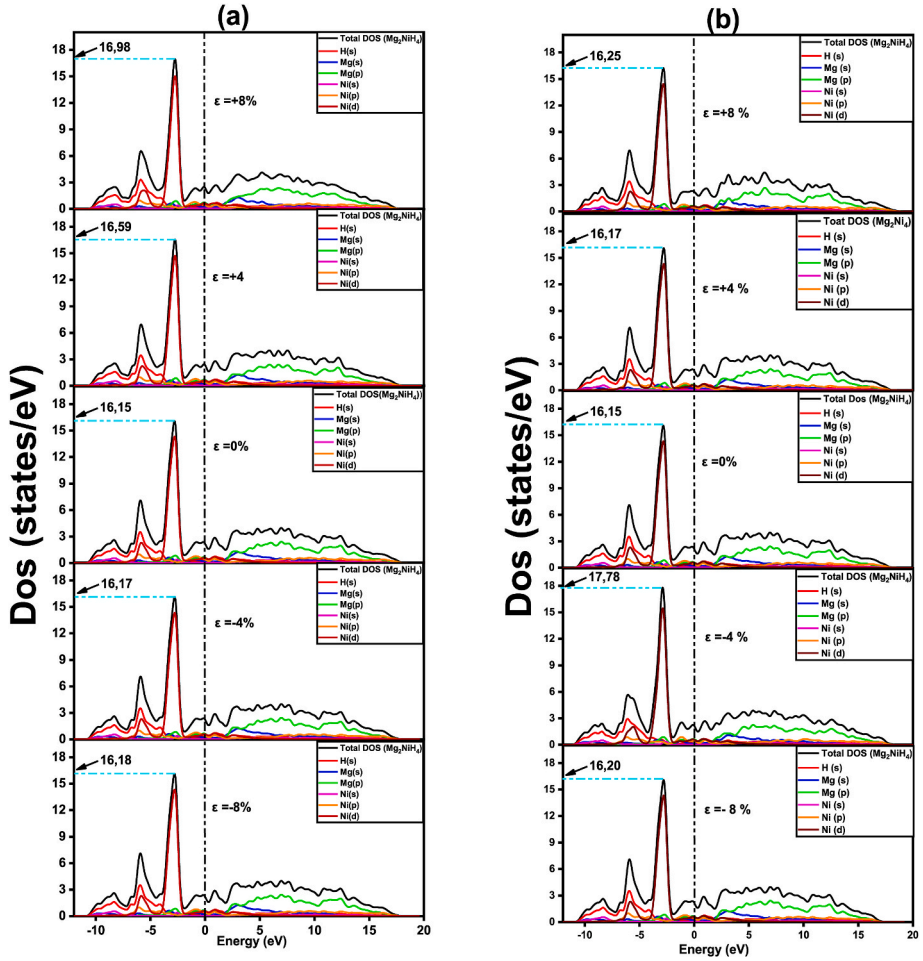

Fig. 5. Partial DOS (PDOS) and total DOS (TDOS) under uniaxial (a) and biaxial (b) strains of Mg_2NiH_4 system.

Mg_2NiH_4, where strain or element substitution modifies the hydrogenation behaviour [25,45]. In this study, we have investigated the Total Density of States (TDOS) and Partial Density of States (PDOS) for the Mg_2NiH_4 system under both uniaxial and biaxial tensile/compressive strain conditions. The Fermi level (E_f) is set to zero and used as a reference point throughout the analysis, allowing us to observe the strain-induced changes in the electronic structure of the material.

As illustrated in Fig. 5a *and* ***5b***, bonding in the Mg_2NiH_4 system involves the *s* orbitals of hydrogen, *s* and *p* orbitals of magnesium, and *s*, *p*, and *d* orbitals of nickel. The contributions of these orbitals are altered when uniaxial or biaxial strains are applied. For example, consider the TDOS peak within the energy range of [−3.94, −1.96] eV. In the presence of uniaxial and biaxial tensile or compressive strains, the TDOS peak is affected accordingly. Specifically, as shown in Fig. 5-a, the TDOS peak increases from 16.15 states/eV in the undeformed state to 16.98 *states/eV* under uniaxial tensile strain ($\varepsilon = +8\%$). Conversely, under uniaxial compression ($\varepsilon = -8\%$), the TDOS peak rises to 16.18 *states/eV*, a smaller increase compared to tensile strain. This difference can be attributed to the Mg_2NiH_4 system's greater resilience to compressive strains compared to tensile strains. On the other hand, as shown in Fig. 5b, the TDOS peak increases to 16.25 states/eV under biaxial tension ($\varepsilon = +8\%$) and reaches 16.20 states/eV under biaxial compression ($\varepsilon = -8\%$). Notably, under biaxial compression of $\varepsilon = -4\%$, the peak rises sharply to 17.78 states/eV. This significant increase in the TDOS peak may explain the observed decrease in ionic conductivity during biaxial compression of $\varepsilon = -4\%$, as illustrated in Fig. 4.

4. Conclusion

This study leverages density functional theory (DFT) with the GGA-PBEsol and GGA-PBE approximation to elucidate the effects of uniaxial and biaxial strains on the Mg_2NiH_4 hydride, offering a thorough analysis of its structural, thermodynamic, mechanical, and electronic properties, as well as its diffusion kinetics and ionic conductivity. The key findings are as follows.

- The structural, thermodynamic, and electronic properties of Mg_2NiH_4 computed in this study align closely with existing literature, confirming the reliability of our theoretical framework.
- Mechanical property assessments demonstrate that while the Mg_2NiH_4 system shows notable resilience to applied strains, it also exhibits some brittleness under specific conditions.
- Strain application enhances the diffusion kinetics of hydrogen atoms within the Mg_2NiH_4 matrix, with a significant reduction of 3.98% in activation energy for hydrogen migration observed under uniaxial compressive strain ($\varepsilon = -8\%$).
- Near-room-temperature hydrogen desorption was achieved through compressive strain, which reduces the enthalpy of formation and facilitates hydrogen release at lower temperatures. Under uniaxial compressive strain (ε = -8%), the decomposition temperature was reduced to approximately 452.41 K, and under biaxial compressive strain (ε = -8%), it decreased further to around 260.24 K. These results highlight the effectiveness of strain-induced modifications in promoting hydrogen desorption closer to ambient conditions.
- Both uniaxial and biaxial strains substantially improve the ionic conductivity of the Mg_2NiH_4 system. For example, uniaxial compressive strain of $\varepsilon = -8\%$ results in a 50.6% increase in ionic conductivity compared to the unstrained hydride.

These results underscore the potential of strategically applied strain to optimize the performance of Mg_2NiH_4 for hydrogen storage applications, paving the way for further research into strain-engineered materials.

CRediT authorship contribution statement

Amine Alaoui-Belghiti: Writing – original draft, Methodology, Investigation, Formal analysis, Conceptualization, Writing – review & editing, Validation, Supervision, Methodology, Investigation, Conceptualization. **Abdelmajid Assila:** Writing – original draft, Validation, Software, Formal analysis. **Ikram Belkoufa:** Software, Funding acquisition, Formal analysis. **Mourad Rkhis:** Validation, Software, Methodology. **Said Laasri:** Conceptualization, Methodology, Validation. **Mouhaydine Tlemçani:** Supervision, Methodology. **El-kebir Hlil:** Supervision, Software, Methodology, Funding acquisition. **Abdelowahed Hajjaji:** Supervision.

Declaration of competing interest

The authors declare that they have no known competing financial interests or personal relationships that could have appeared to influence the work reported in this paper.

References

[1] Li T, Wang B, Cao Y, Liu Z, Wang S, Zhang Q, Sun J, Zhou G. Energy-saving hydrogen production by seawater electrolysis coupling tip-enhanced electric field promoted electrocatalytic sulfion oxidation. Nat Commun 2024;15:6173. https://doi.org/10.1038/s41467-024-49931-5.
[2] Li H, Xiao H. An experimental study on the flame instability of NH3/DME blends with H2 addition. Int J Hydrogen Energy 2024;68:813–22. https://doi.org/10.1016/j.ijhydene.2024.04.302.
[3] Sebbahi S, Assila A, Alaoui Belghiti A, Laasri S, Kaya S, Hlil EK, Rachidi S, Hajjaji A. A comprehensive review of recent advances in alkaline water electrolysis for hydrogen production. Int J Hydrogen Energy 2024;82:583–99. https://doi.org/10.1016/j.ijhydene.2024.07.428.
[4] Ao B, Zhang Z, He Y, Zhao Y. Semiconducting ground-state of three polymorphs of Mg2NiH4 from first-principles calculations. Int J Hydrogen Energy 2013;38:16471–6. https://doi.org/10.1016/j.ijhydene.2013.09.120.
[5] Wang P, Wang Z, Tian Z, Xia C, Yang T, Liang C, Li Q. Enhanced hydrogen absorption and desorption properties of MgH2 with NiS2: the catalytic effect of in-situ formed MgS and Mg2NiH4 phases. Renew Energy 2020;160:409–17. https://doi.org/10.1016/j.renene.2020.07.014.
[6] Jiang J, Zhang S, Huang S, Wang P, Tian H. Density functional theory studies of Yb-, Ca- and Sr-substituted Mg2NiH4 hydrides. Comput Mater Sci 2013;74:55–64. https://doi.org/10.1016/j.commatsci.2013.03.004.
[7] Belkoufa I, Misski B, Alaoui-Belghiti A, Mouyane M, Houivet D, Laasri S, Hlil EK, Hajjaji A. Role of Mg, Ca, and Mo in NaBH4 systems for hydrogen storage applications: ab initio study. Comput Mater Sci 2024;242:113090. https://doi.org/10.1016/j.commatsci.2024.113090.
[8] Belkoufa I, Misski B, Alaoui-Belghiti A, Moslah C, Mouyane M, Houivet D, Laasri S, Hlil EK, Hajjaji A. Improved thermodynamic properties of (Sc, V, Ti, Fe, Mn, Co, and Ni) doped NaBH4 for hydrogen storage: first-principal calculation. Int J Hydrogen Energy 2024;68:481–90. https://doi.org/10.1016/j.ijhydene.2024.04.155.
[9] Yang D, Liang L, Zhang H, Sun Y, Li M, He L. Numerical simulation of the hydrogen charging process in an adsorption storage tank. Int J Hydrogen Energy 2024;68:673–87. https://doi.org/10.1016/j.ijhydene.2024.04.315.
[10] Ferreira O, Fonseca A, Adame CF, Bundaleski N, Robinson R, Teodoro OMND. Advancing hydrogen leak detection: design and calibration of reference leaks. Int J Hydrogen Energy 2024;68:1090–6. https://doi.org/10.1016/j.ijhydene.2024.04.328.
[11] Tran XQ, McDonald SD, Gu Q, Yamamoto T, Shigematsu K, Aso K, Tanaka E, Matsumura S, Nogita K. In-situ investigation of the hydrogen release mechanism in bulk Mg2NiH4. J Power Sources 2017;341:130–8. https://doi.org/10.1016/j.jpowsour.2016.11.105.
[12] Jiang G, Qian Z, Bououdina M, Ahuja R, Liu X. Exploring pristine and Li-doped Mg2NiH4 compounds with potential lithium-storage properties: ab initio insight. J Alloys Compd 2018;746:140–6. https://doi.org/10.1016/j.jallcom.2018.02.290.
[13] Kapustin A, Rakov V. Methodology to evaluate the impact of hybrid cars engine type on their economic efficiency and environmental safety. Transport Res Procedia 2017;20:247–53. https://doi.org/10.1016/j.trpro.2017.01.057.
[14] Rebollar-Pérez G, Carretier E, Lesage N, Moulin P. Vapour permeation of VOC emitted from petroleum activities: application for low concentrations. J Ind Eng Chem 2012;18:1339–52. https://doi.org/10.1016/j.jiec.2012.01.039.
[15] Yamçıçıer Ç, Kürkçü C. Investigation of structural, electronic, elastic, vibrational, thermodynamic, and optical properties of Mg2NiH4 and Mg2RuH4 compounds used in hydrogen storage. J Energy Storage 2024;84:110883. https://doi.org/10.1016/j.est.2024.110883.
[16] Alaoui-Belghiti A, Rkhis M, Laasri S, Hajjaji A, Eljouad M, EL-Otmani R, Hlil E-K. Conception and numerical simulation of heat and mass transfer in a solid state hydrogen storage reactor. Eur Phys J Appl Phys 2019;87:20902. https://doi.org/10.1051/epjap/2019190087.

[17] Rkhis M, Alaoui-Belghiti A, Laasri S, Touhtouh S, Hajjaji A, Hlil EK, Bessais L, Soubane D, Zaidat K, Obbade S. First principle investigation on hydrogen solid storage in Zr1-xNbxNiH3 (x = 0 and 0.1). Int J Hydrogen Energy 2019;44:23188–95. https://doi.org/10.1016/j.ijhydene.2019.07.017.

[18] Assila A, Rkhis M, Alaoui-Belghiti A, Laasri S, Hlil EK, Boughaleb Y, Hajjaji A. Feeling the strain: enhancing the thermodynamics characteristics of magnesium nickel hydride Mg2NiH4 for hydrogen storage applications through strain engineering. Int J Hydrogen Energy 2024;67:651–7. https://doi.org/10.1016/j.ijhydene.2024.04.159.

[19] Assila A, Rkhis M, Sebbahi S, Alaoui Belghiti A, Laasri S, Hlil EK, Zaidat K, Obbade S, Hajjaji A. Improvement of the thermodynamic properties of lithium borohydride LiBH4 by mechanical treatment for hydrogen storage applications: a DFT investigation. Int J Hydrogen Energy 2024;51:72–8. https://doi.org/10.1016/j.ijhydene.2023.10.317.

[20] Mallik N, Hajhemati J, Frégnaux M, Coutancier D, Toby A, Zhang S-T, Hartmann C, Hüsam E, Saleh A, Vincent T, Fournier O, Wilks RG, Aureau D, Félix R, Schneider N, Bär M, Schulz P. Interface defect formation for atomic layer deposition of SnO2 on metal halide perovskites. Nano Energy 2024;126:109582. https://doi.org/10.1016/j.nanoen.2024.109582.

[21] Mouangue RM, Kazet MY, Kuitche A, Ndjaka J-M. Influence of the determination methods of K and C parameters on the ability of weibull distribution to suitably estimate wind potential and electric energy. Int J Renew Energy Dev 2014;3:145–54. https://doi.org/10.14710/ijred.3.2.145-154.

[22] Singer JP, Mayergoyz A, Portet C, Schneider E, Gogotsi Y, Fischer JE. Enhanced volumetric hydrogen storage capacity of porous carbon powders by forming peels or pellets. Microporous Mesoporous Mater 2008;116:469–72. https://doi.org/10.1016/j.micromeso.2008.05.005.

[23] Allouhi A, Zamzoum O, Islam MR, Saidur R, Kousksou T, Jamil A, Derouich A. Evaluation of wind energy potential in Morocco's coastal regions. Renew Sustain Energy Rev 2017;72:311–24. https://doi.org/10.1016/j.rser.2017.01.047.

[24] Bergemann N, Pistidda C, Uptmoor M, Milanese C, Santoru A, Emmler T, Puszkiel J, Dornheim M, Klassen T. A new mutually destabilized reactive hydride system: LiBH4–Mg2NiH4. J Energy Chem 2019;34:240–54. https://doi.org/10.1016/j.jechem.2019.03.011.

[25] Rkhis M, Alaoui-Belghiti A, Laasri S, Touhtouh S, Hlil EK, Bououdina M, Zaidat K, Obbade S, Hajjaji A. Dependence of Mg, Be and Al substitution on the hydrogen storage characteristics of $ZrNiH_3$. Int J Energy Res 2021;45:2292–302. https://doi.org/10.1002/er.5922.

[26] Luo Q, Cai Q, Gu Q, Shi Y, Liu B, Tran XQ, Matsumura S, Zhang T-Y, Nogita K, Lyu T, Li Q, Pan F. Negative thermal expansion and phase transition of low-temperature Mg2NiH4. J Magnesium Alloys 2023;11:3338–49. https://doi.org/10.1016/j.jma.2022.09.012.

[27] Gross KJ, Spatz P, Züttel A, Schlapbach L. Mechanically milled Mg composites for hydrogen storage the transition to a steady state composition. J Alloys Compd 1996;240:206–13. https://doi.org/10.1016/0925-8388(96)02261-X.

[28] Sebbahi S, Assila A, Alaoui Belghiti A, Laasri S, Kaya S, Hlil EK, Rachidi S, Hajjaji A. A comprehensive review of recent advances in alkaline water electrolysis for hydrogen production. Int J Hydrogen Energy 2024;82:583–99. https://doi.org/10.1016/j.ijhydene.2024.07.428.

[29] Alaoui-Belghiti A, Lifi H, Laasri S, Touhtouh S, Hajjaji A. Pyroelectric sensor based on Pb(Mg1/3Nb2/3)1-xTixO3 single crystals for solid state hydrogen storage reactors. Int J Hydrogen Energy 2019;44:15657–64. https://doi.org/10.1016/j.ijhydene.2019.04.022.

[30] Rkhis M, Laasri S, Touhtouh S, Belhora F, Hlil EK, Zaidat K, Obbade S, Hajjaji A. Recent advances in magnesium hydride for solid-state hydrogen storage by mechanical treatment: a DFT study. Int J Hydrogen Energy 2023:S0360319923026575. https://doi.org/10.1016/j.ijhydene.2023.05.267.

[31] Rkhis M, Laasri S, Touhtouh S, Hlil EK, Zaidat K, Obbade S, Hajjaji A. New insights into the electrochemical and thermodynamic properties of AB-type ZrNi hydrogen storage alloys by native defects and H-doping: computational experiments. Int J Hydrogen Energy 2022:S0360319922058311. https://doi.org/10.1016/j.ijhydene.2022.12.115.

[32] Jaafar H, Aymard L, Dachraoui W, Demortière A, Abdellaoui M. Preparation and characterization of mechanically alloyed AB3-type based material LaMg2Ni5Al4 and its solid-gaz hydrogen storage reaction. J Solid State Chem 2018;260:73–9. https://doi.org/10.1016/j.jssc.2018.01.015.

[33] Rkhis M, Laasri S, Touhtouh S, Hlil EK, Hajjaji A. Tailoring the electrochemical performance of olivine phosphate cathode materials for Li-ion batteries by strain engineering: computational experiments. ACS Appl Energy Mater 2023:3c00711. https://doi.org/10.1021/acsaem.3c00711. acsaem.

[34] Salawu SO, Obalalu AM, Fatunmbi EO, Shamshuddin M. Elastic deformation of thermal radiative and convective hybrid SWCNT-Ag and MWCNT-MoS4 magneto-nanofluids flow in a cylinder. Results Mater 2023;17:100380. https://doi.org/10.1016/j.rinma.2023.100380.

[35] Bouhadda Y, Rabehi A, Boudouma Y, Fenineche N, Drablia S, Meradji H. Hydrogen solid storage: first-principles study of ZrNiH3. Int J Hydrogen Energy 2009;34:4997–5002. https://doi.org/10.1016/j.ijhydene.2008.12.082.

[36] Bellosta Von Colbe J, Ares J-R, Barale J, Baricco M, Buckley C, Capurso G, Gallandat N, Grant DM, Guzik MN, Jacob I, Jensen EH, Jensen T, Jepsen J, Klassen T, Lototskyy MV, Manickam K, Montone A, Puszkiel J, Sartori S, Sheppard DA, Stuart A, Walker G, Webb CJ, Yang H, Yartys V, Züttel A, Dornheim M. Application of hydrides in hydrogen storage and compression: achievements, outlook and perspectives. Int J Hydrogen Energy 2019;44:7780–808. https://doi.org/10.1016/j.ijhydene.2019.01.104.

[37] Varnagiris S, Urbonavicius M, Knoks A, Milcius D. Enhanced hydrogen generation in low-range acidic solutions using Mg2NiH4 powders and their mixtures ball-milled with NaCl and fused silica. Int J Hydrogen Energy 2024;50:614–26. https://doi.org/10.1016/j.ijhydene.2023.10.083.

[38] Lu X, Zhang L, Zheng J, Yu X. Construction of carbon covered Mg2NiH4 nanocrystalline for hydrogen storage. J Alloys Compd 2022;905:164169. https://doi.org/10.1016/j.jallcom.2022.164169.

[39] Jiang Y-B, Jiang W, Si N, Wang Z. Hydrogen storage properties of MgH2 + Mg2NiH4–Co/C ternary nanocomposite. Int J Hydrogen Energy 2024;72:258–67. https://doi.org/10.1016/j.ijhydene.2024.05.301.

[40] Myers WR, Wang L-W, Richardson TJ, Rubin MD. Calculation of thermodynamic, electronic, and optical properties of monoclinic Mg2NiH4. J Appl Phys 2002;91:4879–85. https://doi.org/10.1063/1.1454206.

[41] Klebanoff LE, Keller JO. 5 Years of hydrogen storage research in the U.S. DOE metal hydride center of excellence (MHCoE). Int J Hydrogen Energy 2013;38:4533–76. https://doi.org/10.1016/j.ijhydene.2013.01.051.

[42] Satyapal S, Petrovic J, Read C, Thomas G, Ordaz G. The U.S. Department of energy's national hydrogen storage project: progress towards meeting hydrogen-powered vehicle requirements. Catal Today 2007;120:246–56. https://doi.org/10.1016/j.cattod.2006.09.022.

[43] Lakhal M, Bhihi M, Labrim H, Benyoussef A, Naji S, Belhaj A, Khalil B, Abdellaoui M, Mounkachi O, Loulidi M, El kenz A. Kinetic Monte Carlo and density functional study of hydrogen diffusion in magnesium hydride MgH2. Int J Hydrogen Energy 2013;38:8350–6. https://doi.org/10.1016/j.ijhydene.2013.04.157.

[44] Rkhis M, Laasri S, Touhtouh S, Hlil EK, Bououdina M, Ahuja R, Zaidat K, Obbade S, Hajjaji A. Engineering the hydrogen storage properties of the perovskite hydride ZrNiH3 by uniaxial/biaxial strain. Int J Hydrogen Energy 2022;47:3022–32. https://doi.org/10.1016/j.ijhydene.2021.10.237.

[45] Benzidi H, Lakhal M, Benyoussef A, Hamedoun M, Loulidi M, El kenz A, Mounkachi O. First principle study of strain effect on structural and dehydrogenation properties of complex hydride LiBH4. Int J Hydrogen Energy 2017;42:19481–6. https://doi.org/10.1016/j.ijhydene.2017.06.068.

[46] Perdew JP, Burke K, Ernzerhof M. Generalized gradient approximation made simple. Phys Rev Lett 1996;77:3865–8. https://doi.org/10.1103/PhysRevLett.77.3865.

[47] Rutter MJ. C2x: a tool for visualisation and input preparation for Castep and other electronic structure codes. Comput Phys Commun 2018;225:174–9. https://doi.org/10.1016/j.cpc.2017.12.008.

[48] Pingak RK, Harbi A, Moutaabbid M, Johannes AZ, Hauwali NUJ, Bukit M, Nitti F, Ndii MZ. Lead-free perovskites $InSnX_3$ (X = Cl, Br, I) for solar cell applications: a DFT study on the mechanical, optoelectronic, and thermoelectric properties. Mater Res Express 2023;10:095507. https://doi.org/10.1088/2053-1591/acf984.

[49] Yvon K, Schefer J, Stucki F. Structural studies of the hydrogen storage material Mg2NiH4. 1. Cubic high-temperature structure. ACS Publications; 2002. https://doi.org/10.1021/ic50223a006.

[50] Zolliker P, Yvon K, Jorgensen JD, Rotella FJ. Structural studies of the hydrogen storage material magnesium nickel hydride (Mg2NiH4). 2. Monoclinic low-temperature structure. ACS Publications; 2002. https://doi.org/10.1021/ic00240a012.

[51] Noréus D, Werner P-E. The structure of the low temperature phase Mg2NiH4(LT). Mater Res Bull 1981;16:199–206. https://doi.org/10.1016/0025-5408(81)90082-9.

[52] Zhang J, Zhu Y, Yao L, Xu C, Liu Y, Li L. State of the art multi-strategy improvement of Mg-based hydrides for hydrogen storage. J Alloys Compd 2019;782:796–823. https://doi.org/10.1016/j.jallcom.2018.12.217.

[53] Noréus D, Werner P-E. Structural studies of monoclinic Mg2NiD4. J Less Common Met 1984;97:215–22. https://doi.org/10.1016/0022-5088(84)90025-0.

[54] Chen X, Xu J, Yang C, Fang Y, Li W, Zhang Y, Wan Z, Wang X. Thermodynamic and economic study of PEMFC stack considering degradation characteristic. Energy Convers Manag 2021;235:114016. https://doi.org/10.1016/j.enconman.2021.114016.

[55] Wang Y, Liu X, Chen Y, Cai X, Zhou L. High energy ball milling composite modification of Mg2Ni hydrogen storage alloy by graphene and MWCNTs. Int J Hydrogen Energy 2024;50:1562–73. https://doi.org/10.1016/j.ijhydene.2023.10.125.

[56] Selvam P, Viswanathan B, Swamy C, Srinivasan V. Magnesium and magnesium alloy hydrides. Int J Hydrogen Energy 1986;11:169–92. https://doi.org/10.1016/0360-3199(86)90082-0.

[57] Njema H, Boughzala K, Chaabène A, Bouzouita K. Study of the ionic conductivity of Ca6La4(PO4)2(SiO4)4F2 and Ca4La6(SiO4)6F2, comptes rendus. Chimie 2014;17:1237–41. https://doi.org/10.1016/j.crci.2014.02.005.

[58] Rhaiem AB, Hlel F, Guidara K, Gargouri M. Dielectric relaxation and ionic conductivity studies of [N(CH3)4]2Cu0.5Zn0.5Cl4. J Alloys Compd 2008;463:440–5. https://doi.org/10.1016/j.jallcom.2007.09.032.

[59] Masmoudi W, Kamoun S, Ayedi HF, Guidara K. Crystal structure, ionic conductivity and dielectric relaxation studies in the (C5H10N)2BiBr5 compound. Phys B Condens Matter 2012;407:2365–71. https://doi.org/10.1016/j.physb.2012.02.037.

[60] Cioateră N, Pârvulescu V, Rolle A, Vannier RN. Enhanced ionic conductivity of Sm, Gd-doped ceria induced by modification of powder synthesis procedure. Ceram Int 2012;38:5461–8. https://doi.org/10.1016/j.ceramint.2012.03.058.

[61] Louati B, Guidara K, Gargouri M. Dielectric and ac ionic conductivity investigations in the monetite. J Alloys Compd 2009;472:347–51. https://doi.org/10.1016/j.jallcom.2008.04.050.

[62] Blazquez-Alcover I, Rousse G, Alves Dalla Corte D, Badot JC, Grimaud A, Rozier P, Tarascon JM. Improving ionic conductivity by Mg-doping of A2SnO3 (A = Li+, Na+). Solid State Ionics 2017;308:16–21. https://doi.org/10.1016/j.ssi.2017.05.013.

[63] Singh S, Lang L, Dovale-Farelo V, Herath U, Tavadze P, Coudert F-X, Romero AH. MechElastic: a Python library for analysis of mechanical and elastic properties of bulk and 2D materials. Comput Phys Commun 2021;267:108068. https://doi.org/10.1016/j.cpc.2021.108068.

[64] Rkhis M, Anoua R, Alaoui-Belghiti A, Laasri S, Touhtouh S, Hlil EK, Bououdina M, Zaidat K, Obbade S, Hajjaji A. Role of vacancy defects on the dehydrogenation properties of the ternary hydride ZrNiH3: ab-initio insights. Int J Hydrogen Energy 2021;46:13088–96. https://doi.org/10.1016/j.ijhydene.2021.01.100.

[65] Reuss A. Berechnung der Fließgrenze von Mischkristallen auf Grund der Plastizitätsbedingung für Einkristalle. ZAMM - J Appl Math Mech/Z Angew Math Mech 1929;9:49–58. https://doi.org/10.1002/zamm.19290090104.

[66] Hill R. The elastic behaviour of a crystalline aggregate. Proc Phys Soc A 1952;65:349. https://doi.org/10.1088/0370-1298/65/5/307.